Int. J. Adv. Appl. Math. and Mech. 11(4) (2024) 1 – 14 (ISSN: 2347-2529)

Journal homepage: www.ijaamm.com

International Journal of Advances in Applied Mathematics and Mechanics

Analysis on Heat and Mass Transfer in Boundary Layer Non-Newtonian Nanofluid Flow Past a Vertically Stretching Porous Plate with Chemical Reaction, Variable Magnetic Field and Variable Thermal Conductivity

Research Article

Mukonda Danny[1], **Kafunda Tuesday**[2,*] **Christian Kasumo**[1] **Stanley Jere**[1]

[1] *Department of Mathematics and Statistics, Mulungushi University, Zambia.*

[2] *Department of Mathematics, Pan African University Institute of Basic Sciences, Technology and Innovation, Kenya.*

Received 23 March 2024; accepted (in revised version) 15 April 2024

Abstract: The aim of this study is to analyze heat and mass transfer in boundary layer non-Newtonian nanofluid flow past a vertically stretching porous plate which chemical reaction, variable magnetic field and variable thermal conductivity. The system of non-linear partial differential equations governing the flow were solved using finite difference numerical approximation method. The resulting numerical schemes were simulated in MATLAB software. Furthermore, the skin-friction coefficient, Sherwood number, and Nusselt number have been presented in tabular form and discussed. The findings demonstrated that increasing Reynolds and Grashof (for heat and mass transfers) numbers increases velocity profiles while increasing permeability parameter, suction parameter and angle of inclination for the applied magnetic field reduces the velocity profiles of the fluid flow. Temperature of the fluid increases as the angle of inclination, magnetic number,Dufour number, Reynolds number and Eckert number increase but decreases as Prandtl number increases. Induced magnetic field profiles decrease as magnetic Prandtl number and suction parameter increase.Concentration profiles decrease as the chemical reaction parameter and Schmidt number increase but increases as the Soret number increases. The study is significant in cancer therapy, hyperthermia, dynamos, cooling and wound treatment.

MSC: 76A05 • 76D10 • 76M20

Keywords: Boundary Layer • Variable Thermal Conductivity • Heat Transfer • Mass Transfer • Non-Newtonian • Nanofluid • Porous • Variable Magnetic Field; Chemical Reaction

1. Introduction

Recently, hydromagnetic nanofluid flows past stretching plates have attracted reasonable attention to researchers because nanofluids exhibit enhanced heat transfer and energy efficiency characteristics that make them suitable for a wide range of engineering applications.

[1] investigated laminar boundary layer MHD hybrid nanofluid flow and heat transfer driven by mixed convection adjacent to a vertical porous plate in the presence of magnetic induction. The study focused on investigating the effects of nonlinear thermal radiations on energy transport, specifically considering the influences of conduction-radiation and magnetic Prandtl number.The results showed that the induced magnetic field decreased as the Hartmann and

* Corresponding author.

E-mail address(es): dmukonda@mu.edu.zm (Mukonda Danny), kafunda.tuesday@jkuat.ac.ke (Kafunda Tuesday), ckasumo@gmail.com (Christian Kasumo), jere@mu.edu.zm (Stanley Jere).

magnetic Reynolds numbers increased.
[16] investigated the magnetohydrodynamics (MHD) convective nanofluid flow over a vertical stretching sheet considering the thermal radiation and buoyancy effects. Three different base fluids and four different nanoparticles were examined as nanofluid. The governing nonlinear partial differential equations along with the boundary conditions were transformed into a dimensionless form; afterwards, they were solved numerically by the fourth-order Runge–Kutta method with the shooting technique. Parametric investigation was conducted and the influence of various physical parameters, such as magnetic parameter buoyancy parameter, nanoparticle size, nanoparticle concentrations and radiation parameter on velocities and temperature profiles, skin fraction coefficient and reduced Nusselt number are reported. As the results indicated, the reduced Nusselt number had an inverse relation with increasing the nanoparticle concentrations.
[9] conducted an experimental investigation to get insight into convective heat transfer features of the aqueous magnetic fluid flow over a fine wire under the influence of an external magnetic field. The convective heat transfer coefficient of the aqueous magnetic fluid flow around the heated wire was measured in both the uniform magnetic field and the magnetic field gradient. The effects of the external magnetic field strength and its orientation on the thermal behaviors of the magnetic fluids were analyzed. The experimental results showed that the external magnetic field was a vital factor that affected the convective heat transfer performances of the magnetic fluids and the control of heat transfer processes of a magnetic fluid flow could be possible by applying an external magnetic field.
[13] analyzed the mixed convective flow of magneto-nanofluid bounded by a vertical stretchable surface by considering Brownian motion and thermophoretic diffusion effects. The aspects of chemical reaction and activation energy were introduced. Equations governing the locally similar flow were tackled through a numerical approach and the influences of involved parameters on the flow fields were displayed graphically. Buoyancy effects resulting from the temperature and concentration differences accelerated the fluid flow in vertical direction. Brownian motion had no influence on the heat flux from stretching wall. Heat flux from the wall diminishes upon increasing the chemical reaction rate constant. Nanoparticle concentration is directly proportional to the activation energy of chemical reaction and the behavior of Brownian motion on nanoparticle concentration is qualitative opposite to that of thermophoretic force.
[6] investigated the effect of two-dimensional Darcy-Forchheimer flow over second-grade fluid with linear stretching. Heat transfer through convective boundary conditions were considered. Results showed that temperature distribution rises with rise in Dufour number while concentration distribution rises with increase in Soret number. The Forchheimer number and porosity parameter raise the skin friction coefficient. The use of nanofluids in heat exchangers can potentially reduce both volumetric and mass flow rates, thereby leading to an overall decrease in power consumption as investigated in the works of [7].
[10] examined the nanoliquid flow between two horizontal infinite plates. The lower plate is stretchable and permeable. The uniqueness of the flow model is assimilated with the Hall effect, variable thermal conductivity, thermal radiation, and irregular heat source/sink. Transmission of mass is enhanced with the impression of chemical reaction incorporated with activation energy. An increasing behavior is exhibited by the temperature field on escalating the Brownian motion, thermophoresis parameter, variable thermal conductivity, and radiation parameter. For larger values of Schmidt number and chemical reaction parameter, the concentration profile reduces, while a reverse trend is seen for activation energy.
[8] analyzed the impact of Hall current and induced magnetic field on the free convective flow of an electrically conducting, viscous, and incompressible fluid between two non-conducting vertical walls. The findings reviewed that the increase in Hall current led to an increase in both components of velocity, while both components of the induced magnetic field and induced current density decreased [11].
Nanofluids are useful in a wide range of technical applications, including plasma physics, magnetic drug aiming, astronomy and astrophysics, and in electric power generation systems with high efficiency and low emissions [14]. [15] conducted a study on the magneto-hydrodynamics boundary layer heat and mass transfer flow of thermally radiating and dissipative fluid over an infinite plate of vertical orientation with the involvement of induced magnetic field and thermal diffusion.The findings revealed that an increase in the suction parameter leads to a reduction in the values of velocity, temperature, and concentration.
[17] focused on the three-dimensional flow of viscoelastic fluid in the presence of Soret and Dufour effects. Effects of thermophoresis and Brownian motion were considered. Solution expressions of velocity, temperature and nanoparticle concentration were computed via homotopy analysis method. Results were plotted and analyzed for the dimensionless velocities, temperature and nanoparticle concentration. Values of local Nusselt and Sherwood numbers were examined through tabular form. It was observed that Temperature field was enhanced for the larger Brownian motion parameter and an increase in Dufour number gives rise to the temperature and thermal boundary layer thickness.
[19], in this study, one type of applicable analytical method, differential transformation method , was used to evaluate the efficiency and behavior of a straight fin with variable thermal conductivity and heat transfer coefficient. Fins are widely used to enhance heat transfer between primary surface and the environment in many industrial applications. The performance of such a surface is significantly affected by variable thermal conductivity and heat transfer coefficient, particularly for large temperature differences. Results are evaluated for several cases such as: laminar film boiling or condensation, forced convection, laminar natural convection, turbulent natural convection, nucleate boil-

ing, and radiation. The obtained results from DTM are compared with the numerical solution to verify the accuracy of the proposed method. The effects of design parameters on temperature and efficiency are evaluated by some figures. The major aim of the present study, which is exclusive for this article, is to find the effect of the modes of heat transfer on fin efficiency. It has been shown that for radiation heat transfer, thermal efficiency reaches its maximum value.
[5] investigated unsteady hydromagnetic flow of non-Newtonian nanofluid past a stretching sheet in the presence of variable magnetic field and chemical reaction. The system of non-linear partial differential equations governing the flow were approximated using finite difference numerical approximation method. The findings demonstrated that increasing Reynolds number increases velocity profiles while increasing permeability parameter, suction parameter and angle of inclination for the applied magnetic field reduces the velocity profiles of the fluid flow.Temperature of the fluid increases as the angle of inclination, magnetic number, Reynolds number and Eckert number increase but decreases as Prandtl number increases. Induced magnetic field profiles decrease as magnetic Prandtl number and suction parameter increase.Concentration profiles decrease as the chemical reaction parameter and Schmidt number increase but increases as the Soret number increases.
[21] investigated the combined effects of Soret-Dufour and radiation on the unsteady MHD flow of a viscous incompressible and electrically conducting fluid past an impulsively started porous plate embedded in porous medium along with viscous dissipation, chemical reaction, heat generation or absorption with variable temperature, and mass diffusion.
[4] investigated unsteady free convection heat and mass transfer flow past a semi-infinite vertical porous plate numerically by using an explicit finite difference method. The solution of heat and mass transfer flow was studied to examine the velocity, temperature and concentration distribution and it was found that the solution is dependent on several governing parameters, including the magnetic parameter, heat source parameter, Grashof number, modified Grashof number, hall parameter, Prandtl number, Schmidt number, wall temperature and concentration exponent. The effects on the velocity, temperature and concentration profiles for various parameters entering into the problem were separately discussed and shown graphically.
Numerous studies have been conducted on hydromagnetic fluid flows with various factors taken into consideration as illustrated above,however, not much attention has been given to nanofluid flows with boundary layer considering chemical reaction, variable thermal conductivity, variable magnetic field, Dufour effects, Themorphresis, Lorentz force, Joule heating, unsteadiness and viscous dissipation with porous medium.

2. Mathematical formulation

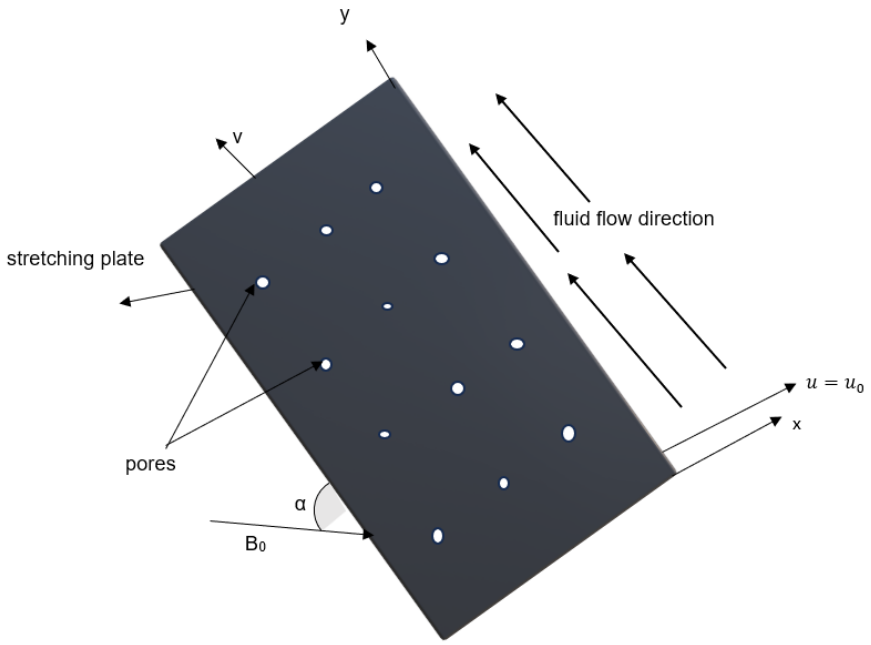

7

Fig. 1. Physical configuration

The present fluid flow problem is a surface driven flow with boundary layer. Figure 1 illustrates the two-dimensional unsteady boundary layer non-Newtonian nanofluid flow past a porous stretching sheet in the vertical direction in the presence of variable magnetic field, chemical reaction and variable thermal conductivity. The ap-

plied magnetic field is given by $\vec{B}_0 cos\alpha \vec{i} + \vec{B}_0 sin\alpha \vec{j}$ where α is the angle of inclination and the total magnetic field is $\vec{B} = \left(B_0 cos\alpha + \vec{B}_x\right)\vec{i} + \left(\vec{B}_0 sin\alpha + \vec{B}_y\right)\vec{j}$ where $\vec{B}_x$ and $\vec{B}_y$ represent the induced magnetic field along x and y directions respectively.
The fluid is being injected and sucked at different intervals with constant velocity u_0 where $u_0 > 0$ represents constant suction velocity and $u_0 < 0$ represents constant injection velocity.
At time $t \leq 0$, the velocity of the nanofluid along y direction is zero, its temperature $T = T_\infty$, its concentration $C = C_\infty$, induced magnetic fields $\vec{H}_x = \vec{H}_y = 0$. When $t > 0$ and $x = 0$ by the no-slip condition of fluid flows, the velocity of the nanofluid along y direction $v = V_\infty$, the temperature of the nanofluid $T = T_{ss}$, its concentration $C = C_{ss}$ and magnetic induction $\vec{H}_x = \vec{H}_y = \vec{H}_0$. As the distances $x \to \infty$ for $t > 0$, the velocity of the nanofluid along x direction is zero, its temperature $T = T_\infty$, its concentration $C = C_\infty$, induced magnetic fields $\vec{H}_x = \vec{H}_y = 0$.

3. Governing Equations

Continuity equation
The fluid flow is assumed to be in two dimensions, the major flow is along y direction and $u = u_0$ is the constant suction/injection velocity along x since the plate is porous. [12], the fluid is assumed to be incompressible, so the continuity equation reduces to

$$\frac{\partial v}{\partial y} = 0 \tag{1}$$

Therefore, velocity, temperature, magnetic induction and concentration are all functions of x and time t only .
[18], **momentum equation along x direction**

$$\frac{\mu_\infty u_0}{K\rho_{n_f}\left(1+\delta\left(T-T_\infty\right)\right)} = -\sigma\left[\left(\vec{B}_0 sin\alpha + \vec{B}_y\right)\left[u_0\left(\vec{B}_0 sin\alpha + \vec{B}_y\right) - v\left(\vec{B}_0 cos\alpha + \vec{B}_x\right)\right]\right] \tag{2}$$

[18], **momentum equation along y direction**

$$\frac{\partial v}{\partial t} + u_0\frac{\partial v}{\partial x} = \frac{\mu_\infty}{\rho_{n_f}\left(1+\delta\left(T-T_\infty\right)\right)}\left(\frac{v}{K} + \frac{\partial^2 v}{\partial x^2}\right) -$$

$$\frac{\sigma}{\rho_{n_f}}\left[-\left(\vec{B}_0 cos\alpha + \vec{B}_x\right)\left[u_0\left(\vec{B}_0 sin\alpha + \vec{B}_y\right) - v\left(\vec{B}_0 cos\alpha + \vec{B}_x\right)\right]\right] + \beta_*^t g\left(T-T_{ss}\right) + \beta_*^c g\left(C-C_{ss}\right) \tag{3}$$

From Navier-Stokes equation along x

$$\frac{-\mu_\infty u_0}{\sigma K\rho_{n_f}\left(1+\delta\left(T-T_\infty\right)\right)\left(\vec{B}_0 sin\alpha + \vec{B}_y\right)} = u_0\left(\vec{B}_0 sin\alpha + \vec{B}_y\right) - v\left(\vec{B}_0 cos\alpha + \vec{B}_x\right) \tag{4}$$

Substituting this relation in the Navier-Stokes equation along y

$$\frac{\partial v}{\partial t} + u_0\frac{\partial v}{\partial x} = \frac{\mu_\infty}{\rho_{n_f}\left(1+\delta\left(T-T_\infty\right)\right)}\left(\frac{v}{K} + \frac{\partial^2 v}{\partial x^2}\right) +$$

$$\left(\frac{\mu_\infty u_0}{K\rho_{n_f}\left(1+\delta\left(T-T_\infty\right)\right)}\right)\left(\frac{\vec{B}_0 cos\alpha + \vec{B}_x}{\vec{B}_0 sin\alpha + \vec{B}_y}\right) + \beta_*^t g\left(T-T_{ss}\right) + \beta_*^c g\left(C-C_{ss}\right) \tag{5}$$

$$\frac{\partial v}{\partial t} + u_0\frac{\partial v}{\partial x} = \frac{\mu_\infty}{\rho_{n_f}\left(1+\delta\left(T-T_\infty\right)\right)}\left(\frac{v}{K} + \frac{\partial^2 v}{\partial x^2} + \frac{u_0}{K}\left(\frac{\vec{H}_0 cos\alpha + \vec{H}_x}{\vec{H}_0 sin\alpha + \vec{H}_y}\right)\right) +$$

$$\beta_*^t g\left(T-T_{ss}\right) + \beta_*^c g\left(C-C_{ss}\right) \tag{6}$$

[2], **energy equation**

$$\frac{\partial T}{\partial t} + u_0\frac{\partial T}{\partial x} = \frac{k_\infty}{\rho_{n_f} c_p}\left[1 + \epsilon\left(\frac{T-T_\infty}{T_{ss}-T_\infty}\right)\right]\left(\frac{\partial^2 T}{\partial x^2}\right) +$$

$$\frac{\mu_\infty}{\rho_{n_f} c_p \left(1+\delta\left(T-T_\infty\right)\right)}\left(\frac{\partial v}{\partial x}\right)^2+\frac{K_t D_m}{c_p C_s}\left(\frac{\partial^2 C}{\partial x^2}\right)+\frac{\sigma\mu_e^2\left[u_0\left(\vec{H}_0 sin\alpha+\vec{H}_y\right)-v\left(\vec{H}_0 cos\alpha+\vec{H}_x\right)\right]^2}{\rho_{n_f} c_p} \tag{7}$$

[3], **magnetic induction equation along x direction**

$$\frac{\partial \vec{H}_x}{\partial t}=\frac{1}{\mu_e\sigma}\left(\frac{\partial^2 \vec{H}_x}{\partial x^2}\right) \tag{8}$$

[3], **magnetic induction equation along y direction**

$$\frac{\partial \vec{B}_y}{\partial t}=\vec{B}_0 cos\alpha\frac{\partial v}{\partial x}+v\frac{\partial \vec{B}_x}{\partial x}+\vec{B}_x\frac{\partial v}{\partial x}-u_0\frac{\partial \vec{B}_y}{\partial x}+\frac{1}{\mu_e\sigma}\left(\frac{\partial^2 \vec{B}_y}{\partial x^2}\right) \tag{9}$$

$$\frac{\partial \vec{H}_y}{\partial t}=\vec{H}_0 cos\alpha\frac{\partial v}{\partial x}+v\frac{\partial \vec{H}_x}{\partial x}+\vec{H}_x\frac{\partial v}{\partial x}-u_0\frac{\partial \vec{H}_y}{\partial x}+\frac{1}{\mu_e\sigma}\left(\frac{\partial^2 \vec{H}_y}{\partial x^2}\right) \tag{10}$$

[22], **concentration equation**

$$\frac{\partial C}{\partial t}=D_m\left(\frac{\partial^2 C}{\partial x^2}\right)-u_0\frac{\partial C}{\partial x}-k_r\left(C-C_\infty\right)+\frac{D_m K_t}{T_m}\left(\frac{\partial^2 T}{\partial x^2}\right) \tag{11}$$

The corresponding initial and boundary conditions are as follows [7]:

$$t\le 0: v=0, T=T_\infty, C=C_\infty, H_x=H_y=0, 0\le x<\infty$$

$$t>0:\left\{\begin{array}{cc} v=V_\infty, T=T_{ss}, C=C_{ss}, H_x=H_y=H_z=H_0 & x=0 \\ v=0, T=T_\infty, C=C_\infty, H_x=H_y=0 & x\to\infty \end{array}\right\} \tag{12}$$

The following non-dimensional variables have been used for the present hydromagnetic flow problem

$$H_x=H_x^* H_0, H_y=H_y^* H_0, x=hx^*,$$

$$t=\frac{h^2 t^*}{\nu_{n_f}}, v=V_\infty v^*, T=T_\infty+\left(T_{ss}-T_\infty\right)T^*, C=C_\infty+\left(C_{ss}-C_\infty\right)C^* \tag{13}$$

Using the above dimensionless variables, the governing equations in non-dimensional form are as follows:

Momentum equation

$$\frac{\partial v^*}{\partial t^*}=-Re.S.\frac{\partial v^*}{\partial x^*}+X.v^*+\frac{\partial^2 v^*}{\partial x^{*2}}+X.S\left(\frac{cos\alpha+\vec{H}_x^*}{sin\alpha+\vec{H}_y^*}\right)+G_r T^*+G_c C^* \tag{14}$$

Energy equation

$$\frac{\partial T^*}{\partial t^*}=-Re.S.\frac{\partial T^*}{\partial x^*}+\frac{1}{P_r}\left(\frac{\partial^2 T^*}{\partial x^{*2}}\right)+E_c\left(\frac{\partial v^*}{\partial x^*}\right)^2+D_f\left(\frac{\partial^2 C^*}{\partial x^{*2}}\right)+M.E_c\left[\left(sin\alpha+\vec{H}_y^*\right)-S\left(cos\alpha+\vec{H}_x^*\right)\right]^2 \tag{15}$$

Magnetic induction equation along x direction

$$\frac{\partial \vec{H}_x^*}{\partial t^*}=\frac{1}{P_{r_m}}\left(\frac{\partial^2 \vec{H}_x^*}{\partial x^{*2}}\right) \tag{16}$$

Magnetic induction equation along y direction

$$\frac{\partial \vec{H}_y^*}{\partial t^*}=Re\left(cos\alpha\frac{\partial v^*}{\partial x^*}+v\frac{\partial \vec{H}_x^*}{\partial x^*}+\vec{H}_x^*\frac{\partial v^*}{\partial x^*}-S.\frac{\partial \vec{H}_x^*}{\partial x^*}\right)+\frac{1}{P_{r_m}}\left(\frac{\partial^2 \vec{H}_y^*}{\partial x^{*2}}\right) \tag{17}$$

Concentration equation

$$\frac{\partial C^*}{\partial t^*}=\frac{1}{S_c}\left(\frac{\partial^2 C^*}{\partial x^{*2}}\right)-Re.S.\frac{\partial C^*}{\partial x^*}-\gamma C^*+S_r\left(\frac{\partial^2 T^*}{\partial x^{*2}}\right) \tag{18}$$

The corresponding initial and boundary conditions are as follows:

$$t^*\le 0: v^*=0, T^*=0, C^*=0, H_x^*=H_y^*=0, 0\le x^*<\infty$$

$$t^*>0:\left\{\begin{array}{cc} v^*=1, T^*=1, C^*=1, H_x^*=H_y^*=1 & x^*=0 \\ v^*=0, T^*=0, C^*=0, H_x^*=H_y^*=0 & x^*\to\infty \end{array}\right\} \tag{19}$$

4. Numerical Solution

The governing equations (14)-(18) are non-linear partial differential equations, therefore cannot be solved analytically. The numerical solutions for velocity,temperature, magnetic induction and concentration profiles are solved using finite difference method subject to the initial and boundary conditions (19). The space and time intervals are fixed at $\Delta x = 0.01$ and $\Delta t = 0.000001$ respectively to ensure stability and convergence of the numerical solution. The equations (14)-(18) at the grid point (j,k) are expressed in difference form , where the spatial partial derivatives are approximated using central difference approximations and temporal partial derivatives are approximated using forward difference approximation as follows :

$$v_j^{k+1} = v_j^k - Re.S.\Delta t\frac{v_{j+1}^k - v_{j-1}^k}{2\Delta y} + X.v_j^k.\Delta t + \frac{v_{j+1}^k - 2v_j^k + v_{j-1}^k}{(\Delta y)^2} +$$

$$X.S.\Delta t\left(\frac{cos\alpha + H_{x_j}^k}{sin\alpha + H_{y_j}^k}\right) + G_r T_j^k + G_c C_j^k$$

$$T_j^{k+1} = T_j^k - Re.S.\Delta t\left(\frac{T_{j+1}^k - T_{j-1}^k}{2\Delta X}\right) + P_r.\Delta t\left(\frac{T_{j+1}^k - 2T_j^k + T_{j-1}^k}{(\Delta x)^2}\right) + D_f\Delta t\left(\frac{C_{j+1}^k - 2C_j^k + C_{j-1}^k}{(\Delta x)^2}\right)$$

$$E_c.\Delta t\left(\frac{v_{j+1}^k - v_{j-1}^k}{2\Delta x}\right)^2 + M.E_c.\Delta t\left[\left(sin\alpha + H_{y_j}^k\right) - S.\left(cos\alpha + H_{x_j}^k\right)\right]^2$$

$$H_{x_j}^{k+1} = H_{x_j}^k + \frac{\Delta t}{P_{r_m}}\left(\frac{H_{x_{j+1}}^k - 2H_{x_j}^k + H_{x_{j-1}}^k}{(\Delta x)^2}\right) \tag{20}$$

$$H_{y_j}^{k+1} = H_{y_j}^k + Re.\Delta t\left(sin\alpha\left(\frac{v_{j+1}^k - v_{j-1}^k}{2\Delta x}\right) + v_j^k\left(\frac{H_{x_{j+1}}^k - H_{x_{j-1}}^k}{2\Delta x}\right) + H_{x_j}^k\left(\frac{v_{j+1}^k - v_{j-1}^k}{2\Delta x}\right)\right) -$$

$$Re.S.\Delta t\left(\frac{H_{y_{j+1}}^k - H_{y_{j-1}}^k}{2\Delta x}\right) + \frac{\Delta t}{P_{r_m}}\left(\frac{H_{x_{j+1}}^k - 2H_{x_j}^k + H_{x_{j-1}}^k}{(\Delta x)^2}\right)$$

$$C_j^{k+1} = C_j^k + \frac{\Delta t}{S_c}\left(\frac{C_{j+1}^k - 2C_j^k + C_{j-1}^k}{(\Delta x)^2}\right) - Re.S.\Delta t\left(\frac{C_{j+1}^k - C_{j-1}^k}{2\Delta x}\right) -$$

$$\gamma C^*.\Delta t + S_r.\Delta t\left(\frac{T_{j+1}^k - 2T_j^k + T_{j-1}^k}{(\Delta x)^2}\right)$$

Subject to the following initial and boundary conditions

$$t \le 0 : v(j,0) = 0, T(j,0) = 0, C(j,0) = 0, H_x(j,0) = H_y(j,0) = 0, 0 \le x < \infty$$

$$t > 0 : \left\{ \begin{array}{ll} v(0,k) = 1, T(0,k) = 1, C(0,k) = 1, H_x(0,k) = H_y(0,k) = 1 & x = 0 \\ v(j,k) = 0, T(j,k) = 0, C(j,k) = 0, H_x(j,k) = H_y(j,k) = 0 & x \to \infty \end{array} \right\} \tag{21}$$

Skin-friction coefficient, Sherwood number and Nusselt number are defined as follows:

$$Nu = \frac{x' T_x}{T_{ss} - T_\infty}$$

$$C_f = \frac{h\tau}{\rho_{nf} V_\infty \nu_{n_f}} \tag{18}$$

$$Sh = \frac{x' C_x}{C_{ss} - C_\infty}$$

where $T_x = -\left(\frac{\partial T}{\partial x}\right)_{x=0} = -\left(\frac{T_{ss}-T_\infty}{h}\right)\left(\frac{\partial T^*}{\partial x^*}\right)_{x^*=0}$, $\tau = \mu_{nf}\left(\frac{\partial v}{\partial x}\right)_{x=0} = \mu_{nf}\left(\frac{V_\infty}{h}\right)\left(\frac{\partial v^*}{\partial x^*}\right)_{x^*=0}$ where $\mu_{nf} = \frac{\mu_\infty}{(1+\delta(T-T_\infty))}$ and $C_x = -\left(\frac{\partial C}{\partial x}\right)_{x=0} = -\left(\frac{C_{ss}-C_\infty}{h}\right)\left(\frac{\partial C^*}{\partial x^*}\right)_{x^*=0}$
Substituting these in (18) to obtain

$$Nu.Re_x^{-1} = -\left(\frac{\partial T^*}{\partial x^*}\right)_{x^*=0}, C_f = \left(\frac{\partial v^*}{\partial x^*}\right)_{x^*=0}, Sh.Re_x^{-1} = -\left(\frac{\partial C^*}{\partial x^*}\right)_{x^*=0} \tag{19}$$

Expressing Nusselt number, Skin Friction coefficient and Sherwood number in finite difference form using forward difference approximations.

$$Nu.Re_x^{-1} = -\left(\frac{T_{j+1}^k - T_j^k}{\Delta x}\right)_{x=0}$$

$$C_f = \left(\frac{v_{j+1}^k - v_j^k}{\Delta x}\right)_{x=0} \tag{20}$$

$$Sh.Re_x^{-1} = -\left(\frac{C_{j+1}^k - C_j^k}{\Delta x}\right)_{x=0}$$

5. Results and Discussion

The physical significance of the boundary layer flow problem has been analysed by graphically representing and discussing the effects of different dimensionless parameters on the flow variables. Additionally, the skin-friction coefficient, Sherwood number, and Nusselt number have been presented in tabular form and discussed. The numerical solutions have been evaluated by fixing the values of various dimensionless parameters involved in the problem such as $Re = 1$,$Pr = 0.71$, $S = 1$, $M = 1$,$Gr = 1$, $Gc = 1$, $Df = 1$, $P_{r_m} = 0.01$, $X = 2$, $Ec = 0.03$, $\alpha = \frac{\pi}{9}$,$Sc = 0.22$, $Sr = 0.2$ and $\gamma = 1$.

Figure 2 demonstrates that an increase in the Reynolds number (Re) results in a corresponding increase in the velocity profiles. As the Reynolds number increases, the viscous forces in the fluid decrease, causing the fluid particles to flow at a higher velocity due to reduced resistance.

Figure 3 clearly demonstrates that increasing the permeability parameter (X) results in a decrease in the velocity profiles. A higher value of the permeability parameter signifies an increased porosity within the stretching sheet, resulting in a decrease in the velocity at which the fluid flows. As a result, the heightened permeability creates greater retardation to the movement of the fluid, causing a reduction in fluid velocity due to a thinner boundary layer of velocity [23].

Figure 4 demonstrates that an increase in the suction parameter results in a drop in fluid velocity when the value of $S < 0$. Conversely, an increase in the injection parameter leads to an increase in fluid velocity profiles when the value of $S > 0$. When $(S < 0)$, it indicates that fluid particles are being extracted from the flow system. This causes fluid particles to be drawn in the horizontal direction, resulting in a decrease in the major flow velocity in the y-direction. This occurs because some of the fluid's kinetic energy is redirected into the horizontal direction. However, when the value of $S > 0$, it indicates the addition of more fluid particles to the fluid flow system. This results in an increase in the velocity of the flow in the y-direction, as a larger number of fluid particles now contribute to the total flow.

Figure 5 demonstrates that increasing the angle of inclination of the applied magnetic field leads to a decrease in the velocity of the fluid. The reason for this is that raising the angle of inclination amplifies the applied magnetic field. In general, an augmentation in the magnetic field produces a counteracting force to the movement, known as the Lorentz force. This force exhibits a propensity to reduce the velocity of the fluid.

Figure 6 demonstrates that an increase in the Grashof number for heat transfer results in a corresponding increase in the velocity profiles. The Grashof number for heat transfer quantifies the relative strength of thermal buoyant forces compared to viscous forces. Consequently, elevating the Grashof number for heat transfer diminishes the influence of viscous forces while enhancing the thermal buoyancy force. As a result, the nanofluid gains the capacity to flow at a greater velocity.

Figure 7 demonstrates that an increase in the Grashof number for mass transfer results in a corresponding rise in velocity profiles. The Grashof number for mass transfer quantifies the relationship between the buoyant forces of species and the viscous forces. Hence, elevating the Grashof number for mass transfer results in a decrease in the viscous forces that contributes to the velocity of the nanofluid past the porous stretching plate.

Figure 8 demonstrates a direct relationship between the Eckert number and the temperature of the nanofluid, indicating that as the Eckert number increases, the temperature of the nanofluid also increases. The Eckert number is a measure of the ratio between the kinetic energy and enthalpy of a nanofluid flow. An increase in the Eckert number signifies that the kinetic energy of the fluid surpasses its enthalpy, resulting in convective heating. This occurs as the fluid's kinetic energy is converted into thermal energy while flowing past a stretching plate. The thermal energy is generated as internal energy or heat, resulting in an increase in the fluid's temperature.

Figure 9 demonstrates that an increase in the Dufour number results in increased temperature profiles. The Dufour number represents the heat flux resulting from a gradient in mass concentration. Raising this value indicates that the fluid experiences significant heating, resulting in the generation of thermal flux and subsequently leading to an augmentation in the thickness of the thermal boundary layer. Consequently, the temperature of the fluid increases.

Figure 10 demonstrates a positive relationship between the magnetic number and the fluid temperature, indicating that an increase in the magnetic number results in a higher fluid temperature. The magnetic number represents the ratio of magnetic forces to fluid inertia forces. Therefore, an increase in the magnetic parameter leads to an increase in magnetic forces and a decrease in inertia forces. When fluid particles in motion come into contact with a stronger magnetic field, result in the generation of an induced electric current. The fluid particles then collide with the charged particles of the current, causing vibrations and generating thermal energy in the form of heat. Consequently, enhancing the magnetic number results in a rise in the fluid's temperature [5].

Figure 11 demonstrates that higher Reynolds numbers leads to increased temperature profiles. As Reynolds number is defined as the ratio of inertia forces to viscous forces, an increase in Reynolds number indicates a decrease in the significance of viscous forces. A reduction in viscous forces leads to enhanced fluid particle motion and the generation of heat through high-velocity particle collisions, resulting in an increase in fluid temperature.

Figure 12 demonstrates the impact of the Prandtl number on temperature profiles.The Prandtl number's relevance resides in its impact on the heat transfer properties of a fluid, since it determines the manner in which heat is transmitted within the fluid and between the fluid and its surroundings. An inverse relationship is noticed between the Prandtl number and the temperature of the fluid, where an increase in the Prandtl number results in a drop in the fluid's temperature. The Prandtl number is defined as the ratio of momentum diffusivity to thermal diffusivity. Higher Prandtl number decreases the thermal diffusivity and increase the viscosity of the fluid, resulting in a decreased thermal boundary layer and a subsequent reduction in the fluid's temperature.

Figure 13 demonstrates that increasing magnetic Prandtl number leads to a decrease in induced magnetic field long y direction.When the magnetic Prandtl number, which represents the ratio of momentum diffusivity to magnetic diffusivity, increases, it indicates a decrease in magnetic diffusivity. Consequently, the induced magnetic field generated by the motion of the conducting medium decreases, resulting in a reduction of induced magnetic profiles along the y-direction.

Figure 14 demonstrates that an increase in the Reynolds number results in a corresponding rise in the magnetic field profiles induced along the y-axis. The Reynolds number represents the ratio of inertia forces to viscous forces. Therefore, a rise in the Reynolds number indicates a decrease in viscous forces, resulting in enhanced interaction between the fluid and the magnetic field. Consequently, this leads to an increase in the induced magnetic field.

Figure 15 demonstrates that an increase in the suction/injection parameter leads to a decrease in induced magnetic field profiles. The suction parameter is the ratio of the suction velocity to the uniform velocity of the stretching plate. Increasing this parameter results in a drop in the velocity of the stretching plate. Since this flow is boundary layer surface driven, it indicates a decrease in the velocity of the fluid. This results in a reduced interaction between the fluid and the magnetic field, hence causing a drop in the profiles of the induced magnetic field.

Figure 16 demonstrates that an increase in the magnetic Prandtl number results in a reduction in the profiles of the induced magnetic field. The magnetic Prandtl number represents the ratio of momentum diffusivity to magnetic diffusivity. As a result, an increase in the magnetic Prandtl number indicates a lower rate of magnetic diffusion, as the viscosity diffusion rate becomes more dominant. Consequently, this results in a decrease in the profiles of the induced magnetic field.

Figure 17 demonstrates a clear inverse relationship between the concentration of the nanofluid and the Schmidt number in that increasing Schmidt number leads to decrease in the concentration profiles. The Schmidt number represents the ratio of momentum diffusivity to mass diffusivity of particles. Increasing this parameter results in a decrease in mass diffusivity, which in turn leads to a drop in the concentration profiles of the nanofluid.

Figure 18 demonstrates that increasing Soret number increases concentration profiles. The Soret number determines the effect of the temperature gradients inducing significant mass diffusion effects. Increasing Soret number generates mass flux that leads to an increase in the mass boundary layer thickness. Therefore, an increase in the Soret number results to an increase in the concentration of the fluid.

Figure 19 demonstrates that an increase in the chemical reaction parameter results in a reduction in the concentration of the fluid particles.A greater chemical reaction parameter signifies that the chemical reaction advances more rapidly compared to the fluid movement. Consequently, a greater amount of reactants is used or transformed into products within a specific timeframe, resulting in a reduction in the concentration of the reactants in the fluid.During a chemical reaction, the concentration of the reactant species diminishes as they undergo chemical transformations to produce the products. During the course of the chemical reaction, the molecules of the reactants come into contact

and undergo a reaction, resulting in the creation of products. Consequently, the concentration of the reactive species diminishes due to their conversion into new products, resulting in a reduction in the chemical molecular diffusivity.

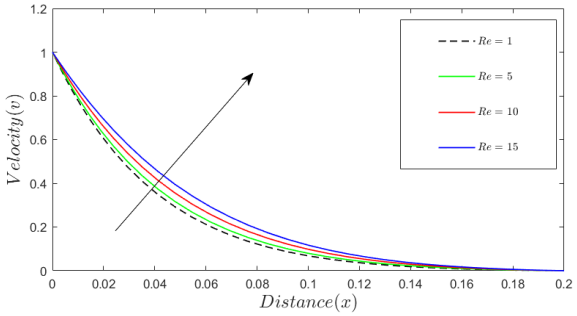

Fig. 2. Velocity profiles for different values of Re l

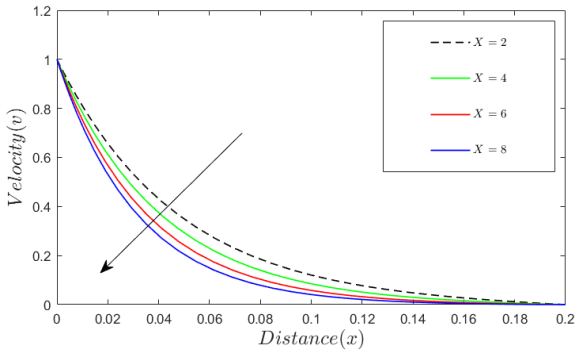

Fig. 3. Velocity profiles for different values of X

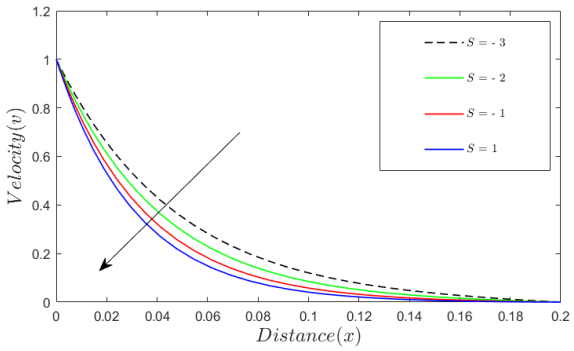

Fig. 4. Velocity profiles against varying values of S

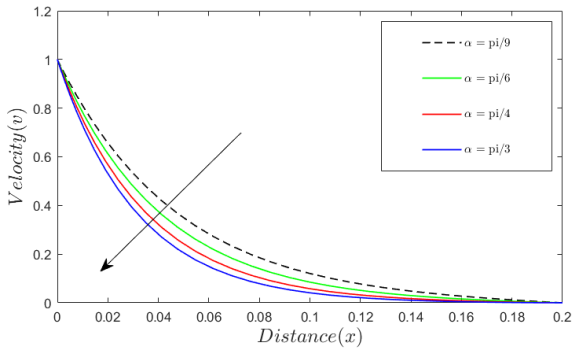

Fig. 5. Velocity profiles for different values of α

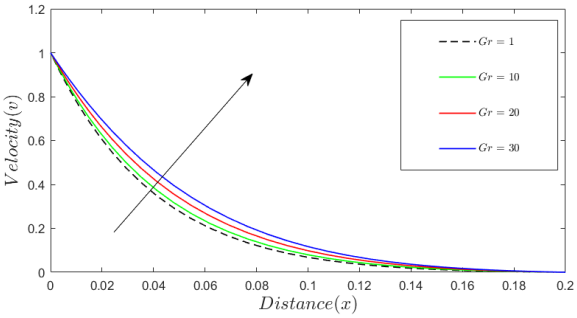

Fig. 6. Velocity profiles for different values of Gr

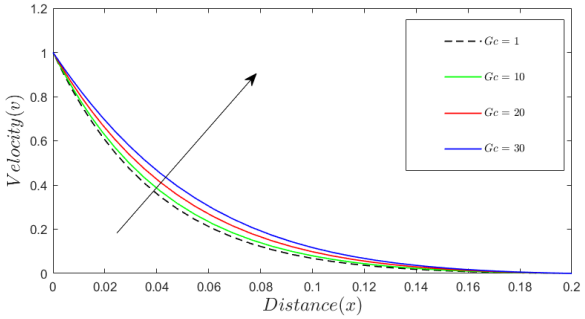

Fig. 7. Velocity profiles for different values of Gc

Table 1 shows that as Reynolds number increases, the skin-friction coefficient reduces in magnitude. This is because as Reynolds number increases, the coefficient of dynamic viscosity reduces and since the skin friction coefficient is directly proportional to the coefficient of dynamic viscosity, then the skin-friction also reduces.At low Reynolds numbers, the viscous forces dominate over the inertia forces. The flow is smooth and ordered, with fluid particles moving in well-defined layers. The skin friction coefficient, which measures the frictional drag of the fluid on a solid surface, tends to be relatively higher because of the strong interaction between the fluid and the solid surface. The shear stress between fluid layers is significant, resulting in a higher skin friction coefficient. Additionally, increasing the values of permeability parameter, suction/injection parameter and angle of inclination for the applied magnetic field decreases the skin-friction coefficient in magnitude. Table 2 shows that increasing Schmidt number reduces Sherwood number while increasing Soret number and chemical reaction parameter increases Sherwood number.The chemical reaction parameter enhances mass transfer by generating concentration gradients through rapid chemical reactions, while the Soret number enhances mass transfer by inducing concentration gradients due to thermal diffu-

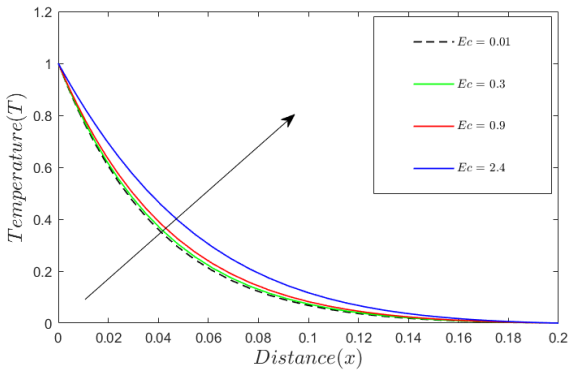

Fig. 8. Temperature profiles for different values of Ec

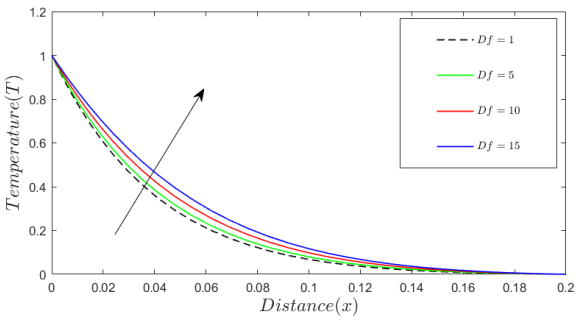

Fig. 9. Temperature profiles for different values of Df

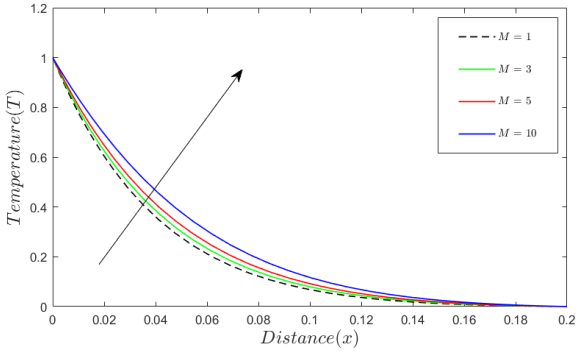

Fig. 10. Temperature profiles for different values of M

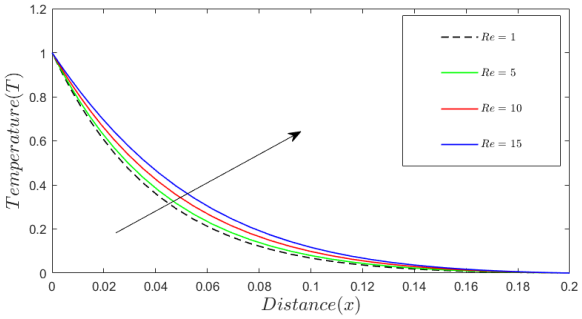

Fig. 11. Temperature profiles for different values of Re

Table 1. Results of Skin-friction coefficient for various physical parameters.

Re	X	S	α	-Cf
1	2	1	$\frac{\pi}{9}$	4.22051
5	2	1	$\frac{\pi}{9}$	2.63383
10	2	1	$\frac{\pi}{9}$	1.32005
15	2	1	$\frac{\pi}{9}$	0.57334
	4	1	$\frac{\pi}{9}$	3.96262
	6	1	$\frac{\pi}{9}$	3.70168
	8	1	$\frac{\pi}{9}$	3.43761
		2	$\frac{\pi}{9}$	3.65790
		3	$\frac{\pi}{9}$	3.13618
		4	$\frac{\pi}{9}$	2.65460
			$\frac{\pi}{6}$	4.19410
			$\frac{\pi}{4}$	4.14642
			$\frac{\pi}{3}$	4.08241

sion effects. Table 3 shows that increasing the values of the angle of inclination, Eckert number and magnetic number increases the Nusselt number by facilitating an increase in convective heat transfer due to the increased kinetic energy of the flow.. However, increasing the values of suction/injection parameter and Prandtl number reduces the Nusselt number. This is because increasing the angle of inclination, Eckert number and magnetic number increases rate of heat transfer thereby increasing thermal boundary layer thickness while increasing suction/injection parameter and Prandtl number leads to thinning of the thermal boundary layer thickness.Increasing Nusselt number signifies the presence of convective heat transfer at the boundary in the fluid whereas decreasing Nusselt number signifies conductive heat transfer at the boundary is dominant.

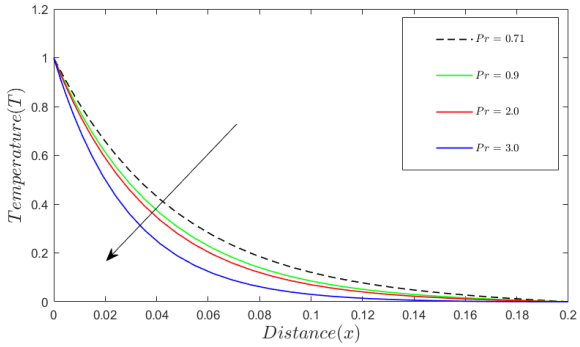

Fig. 12. Temperature profiles for different values of Pr

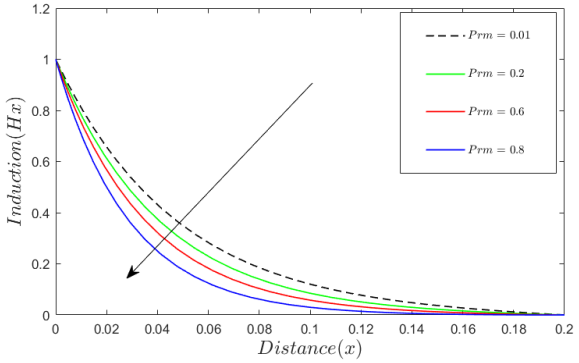

Fig. 13. Induced magnetic profiles (Hx) for different values of Prm

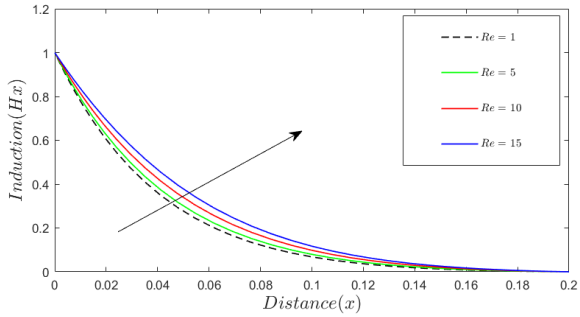

Fig. 14. Induced magnetic profiles (Hx) for different values of Re

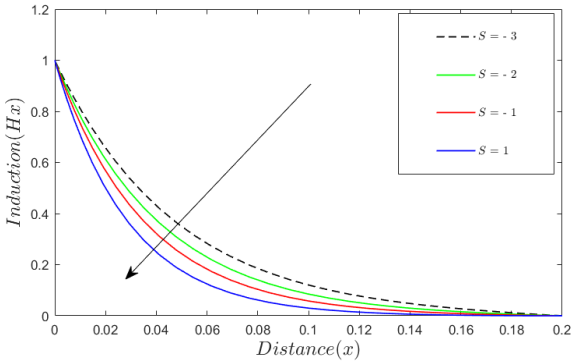

Fig. 15. Induced magnetic profiles (Hx) for different values of S

Table 2. Results of Sherwood number for various physical parameters.

Sc	Sr	γ	Shw
0.22	0.2	1	-4.9051
0.66	0.2	1	-4.73928
0.88	0.2	1	-4.65858
1.0	0.2	1	-4.61562
	1	1	-4.97794
	3	1	-5.14903
	5	1	-5.32011
		3	-4.93877
		5	-4.96797
		7	-4.99710

6. Validation of Results

In validating the numerical code for the accuracy of the computed results, effects of varying Magnetic number, Prandtl number, Suction parameter, Schmidt number and chemical reaction parameter on skin-friction coefficient, Nusselt number and Sherwood number are compared with the results obtained by [20] who investigated chemical reaction and radiation effects on MHD flow of Oldroyd-B fluid through porous medium past an exponentially stretching sheet with heat sink.

It can be observed that the results are in excellent agreement.

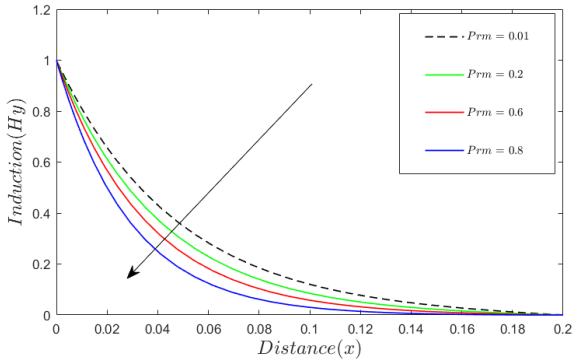

Fig. 16. Induced magnetic profiles (Hy) for different values of Prm

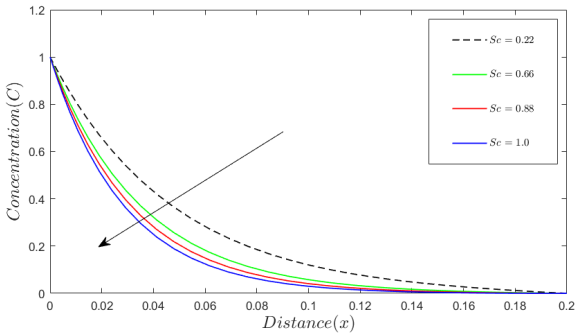

Fig. 17. Concentration profiles (C) for different values of Sc

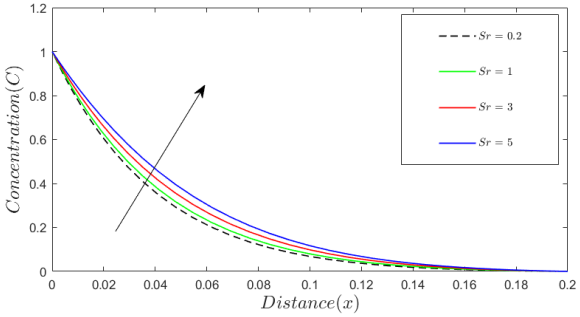

Fig. 18. Concentration profiles (C) for different values of Soret number

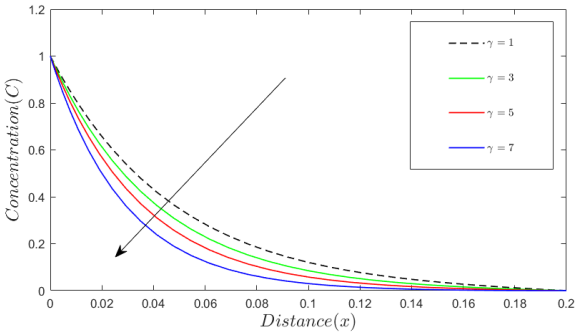

Fig. 19. Concentration profiles (C) for different values of γ

Table 3. Results of Nusselt number for various physical parameters.

α	S	Pr	Ec	M	Nu
$\frac{\pi}{9}$	1	0.71	0.01	1	-4.60415
$\frac{\pi}{6}$	1	0.71	0.01	1	-4.60437
$\frac{\pi}{4}$	1	0.71	0.01	1	-4.60457
$\frac{\pi}{3}$	1	0.71	0.01	1	-4.60463
	2	0.71	0.01	1	-4.27284
	3	0.71	0.01	1	-3.95466
	4	0.71	0.01	1	-3.64966
		0.9	0.01	1	-4.50465
		2	0.01	1	-3.96632
		3	0.01	1	-3.52033
			0.3	1	-4.14100
			0.9	1	-4.24345
			2.4	1	-4.54232
				3	-4.60365
				5	-4.60373
				10	-4.60192

Table 4. Comparison of the effects of varying parameters on skin-friction coefficient.

M	Pr	S	Sc	γ	-C.f for [20]	Present study
0	1	-0.5	0.22	1	1.281808	1.281799
2	5	-0.5	0.22	1	1.912620	1.912620
2	1	-0.2	0.22	1	1.912620	1.912620
2	1	0.5	0.66	1	1.912620	1.912620
2	1	0.5	0.22	3	1.912620	1.912620

Table 5. Comparison of the effects of varying parameters on Nusselt number.

M	Pr	S	Sc	γ	Nu for [20]	Present study
0	1	-0.5	0.22	1	0.753562	0.753559
2	5	-0.5	0.22	1	1.555223	1.555222
2	1	-0.2	0.22	1	0.690708	0.690707
2	1	0.5	0.66	1	0.526591	0.526890
2	1	0.5	0.22	3	0.444567	0.444566

Table 6. Comparison of the effects of varying parameters on Sherwood number.

M	Pr	S	Sc	γ	Sh for [20]	Present study
0	1	-0.5	0.22	1	0.621762	0.621761
2	5	-0.5	0.22	1	0.586776	0.586776
2	1	-0.2	0.22	1	0.586776	0.586776
2	1	0.5	0.66	1	0.586776	0.586776
2	1	0.5	0.22	3	0.586776	0.586776

7. Conclusion

In this study, the problem of heat and mass transfer in s boundary layer non-Newtonian nanofluid flow past a vertically stretching porous plate which chemical reaction, variable magnetic field and variable thermal conductivity has been examined. Results have shown that the rate of mass transfer reduces with an increase in Schmidt number while increases with an increase in Soret number and chemical reaction parameter.The rate of heat transfer increases with an increase in the values of the angle of inclination, Eckert number and magnetic number while reduces with an increase in the values of suction/injection parameter and Prandtl number.

Data Availability

The data used to support the findings of this study are included within the article. The results generated using MATLAB code are presented in tables and figures and also in results and discussion of this manuscript.

Conflicts of Interest

The authors declare they have no conflicts of interest regarding publication of this article.

Funding Statement

The authors express their gratitude to Mulungushi University, (Zambia) for their timely support throughout the conduct of the research.

Acknowledgment

The authors acknowledge Nictor Mwamba and Albert Chilonga for the meaningful academic support rendered during writing of this article.

References

[1] Alharbi, S. O. (2021). Impact of hybrid nanoparticles on transport mechanism in magnetohydrodynamic fluid flow exposed to induced magnetic field. *Ain Shams Engineering Journal*, 12(1):995–1000.

[2] Amos, E. and Uka, U. A. (2022). Hydromagnetic nanofluid flow over an exponentially stretching sheet in the presence of radiation and nonuniform heat generation. *IOSR Journal of Mathematics*, 18(1):31–43.

[3] Bhattacharyya, A., Sharma, R., Hussain, S., Chamkha, A., and Mamatha, E. (2022). A numerical and statistical approach to capture the flow characteristics of maxwell hybrid nanofluid containing copper and graphene nanoparticles. *Chinese Journal of Physics*, 77:1278–1290.

[4] Iva, L., Hasan, M., Paul, S., and Mondal, R. (2018). Mhd free convection heat and mass transfer flow over a vertical porous plate in a rotating system with hall current, heat source and suction. *International journal of advances in applied mathematics and mechanics*, 6(1):49–64.

[5] Kafunda, T. et al. (2023). Unsteady hydromagnetic non-newtonian nanofluid flow past a porous stretching sheet in the presence of variable magnetic field and chemical reaction. *Journal of Applied Mathematics and Physics*, 11(9):2545–2567.

[6] Khan, A. A., Naeem, S., Ellahi, R., Sait, S. M., and Vafai, K. (2020). Dufour and soret effects on darcy-forchheimer flow of second-grade fluid with the variable magnetic field and thermal conductivity. *International Journal of Numerical Methods for Heat & Fluid Flow*, 30(9):4331–4347.

[7] Kinyanjui, M. and Onyango, E. R. (2022). Hydromagnetic surface driven flow between two parallel vertical plates in the presence of chemical reaction and induced magnetic field. *Global Journal of Pure and Applied Mathematics*, 18(1):583–612.

[8] Kumar, D., Singh, A., and Kumar, D. (2018). Effect of hall current on the magnetohydrodynamic free convective flow between vertical walls with induced magnetic field. *The European Physical Journal Plus*, 133(5):207.

[9] Li, Q. and Xuan, Y. (2009). Experimental investigation on heat transfer characteristics of magnetic fluid flow around a fine wire under the influence of an external magnetic field. *Experimental Thermal and Fluid Science*, 33(4):591–596.

[10] Lv, Y.-P., Shaheen, N., Ramzan, M., Mursaleen, M., Nisar, K. S., and Malik, M. (2021). Chemical reaction and thermal radiation impact on a nanofluid flow in a rotating channel with hall current. *Scientific Reports*, 11(1):19747.

[11] Masoud Hosseini, S., Safaei, M. R., Estellé, P., and Hadi Jafarnia, S. (2020). Heat transfer of water-based carbon nanotube nanofluids in the shell and tube cooling heat exchangers of the gasoline product of the residue fluid catalytic cracking unit. *Journal of Thermal Analysis and Calorimetry*, 140(1):351–362.

[12] Megahed, A. M., Ghoneim, N. I., Reddy, M. G., and El-Khatib, M. (2021). Magnetohydrodynamic fluid flow due to an unsteady stretching sheet with thermal radiation, porous medium, and variable heat flux. *Advances in Astronomy*, 2021.

[13] Mustafa, M., Khan, J. A., Hayat, T., and Alsaedi, A. (2017). Buoyancy effects on the mhd nanofluid flow past a vertical surface with chemical reaction and activation energy. *International Journal of Heat and Mass Transfer*, 108:1340–1346.

[14] Mwamba, N., Okelo Abonyo, J., Awuor, K. O., et al. (2023). Effects of thermal radiation and chemical reaction on hydromagnetic fluid flow in a cylindrical collapsible tube with an obstacle. *International Journal of Mathematics and Mathematical Sciences*, 2023.

[15] Poddar, S., Islam, M. M., Ferdouse, J., Alam, M., et al. (2021). Characteristical analysis of mhd heat and mass transfer dissipative and radiating fluid flow with magnetic field induction and suction. *SN Applied Sciences*, 3(4):1–17.

[16] Pourmehran, O., Rahimi-Gorji, M., and Ganji, D. (2016). Heat transfer and flow analysis of nanofluid flow induced by a stretching sheet in the presence of an external magnetic field. *Journal of the Taiwan Institute of Chemical Engineers*, 65:162–171.

[17] Ramzan, M., Inam, S., and Shehzad, S. (2016). Three dimensional boundary layer flow of a viscoelastic nanofluid with soret and dufour effects. *Alexandria Engineering Journal*, 55(1):311–319.

[18] Reddy, K. V. and Reddy, G. V. R. (2022). Outlining the impact of melting on mhd casson fluid flow past a stretching sheet in a porous medium with radiation. *Biointerface Research in Applied Chemistry*, 13:1–14.

[19] Sadri, S., Raveshi, M. R., and Amiri, S. (2012). Efficiency analysis of straight fin with variable heat transfer coefficient and thermal conductivity. *Journal of Mechanical Science and Technology*, 26:1283–1290.

[20] Salah, F. and Sidahmed, A. O. (2022). Chemical reaction and radiation effects on mhd flow of oldroyd-b fluid through porous medium past an exponentially stretching sheet with heat sink. *Journal of Applied Mathematics*, 2022.

[21] Shukla, A. and Dube, S. K. (2022). Numerical simulation of changes in soret-dufour number, radiation, chemical reaction and viscous dissipation on unsteady mhd flow past an inclined porous plate embedded in porous medium with heat generation or absorption. *International Journal of Advances in Applied Mathematics and Mechanics*, 10:15–26.

[22] Yadav, A. S., Khare, R. K., and James, M. (2019). Fluid flow through porous medium in a horizontal channel in inclined magnetic field. *Journal of Applied Science and Computati-ons*, 6(1):1223–1226.

[23] Zaidi, H. N., Yousif, M., and Nazia Nasreen, S. (2020). Effects of thermal radiation, heat generation, and induced magnetic field on hydromagnetic free convection flow of couple stress fluid in an isoflux-isothermal vertical channel. *Journal of Applied Mathematics*, 2020.